

# Neutron Star Mergers and Nucleosynthesis of Heavy Elements

**F.-K. Thielemann<sup>1,2</sup>, M. Eichler<sup>3</sup>, I.V. Panov<sup>4,5</sup>,  
and B. Wehmeyer<sup>6</sup>**

<sup>1</sup>Department of Physics, University of Basel, CH-4056 Basel, Switzerland; email: f-k.thielemann@unibas.ch

<sup>2</sup>GSI Helmholtzzentrum für Schwerionenforschung GmbH, D-64291 Darmstadt, Germany

<sup>3</sup>Institut für Kernphysik, Technische Universität Darmstadt, D-64289 Darmstadt, Germany; email marius.eichler@theorie.ikp.physik.tu-darmstadt.de

<sup>4</sup>Institute for Theoretical and Experimental Physics of NRC Kurchatov Institute, Moscow, Russia; email: panov\_iv@itep.ru

<sup>5</sup>Sternberg Astronomical Institute, M.V. Lomonosov State University, Universitetskij pr., 13, 119234, Moscow, Russia

<sup>6</sup>Department of Physics, North Carolina State University, Raleigh, NC, 27695-8202, USA; email: bwehmey@ncsu.edu

Xxxx. Xxx. Xxx. Xxx. 2017. 67:1–24

This article's doi:  
10.1146/((please add article doi))

Copyright © 2017 by Annual Reviews.  
All rights reserved

## Keywords

compact binary / neutron star mergers, r-process, nuclear properties far from stability, chemical evolution of galaxies

## Abstract

Neutron star mergers have been predicted since the 1970's, supported by the discovery of the binary pulsar and the observation of its orbital energy loss, consistent with General Relativity. They are considered as nucleosynthesis sites of the rapid neutron-capture process (r-process), being responsible for making about half of all heavy elements beyond Fe and being the only source of elements beyond Pb and Bi. Detailed nucleosynthesis calculations based on the decompression of neutron-star matter are consistent with solar r-process abundances of heavy nuclei. More recently neutron star mergers have also been identified with short duration Gamma-Ray Bursts via their IR afterglow, only explainable by the opacities of heavy (rather than only Fe-group) nuclei. Two other observations support rare events like neutron star mergers as a dominant scenario for the production of the heaviest r-process nuclei: (a) The discrepancy between the latest admixtures of two long-lived radioactivities ( $^{60}\text{Fe}$  and  $^{244}\text{Pu}$ ) found on earth seems to exclude the origin of the latter from core collapse supernovae. (b) The ratio of  $[\text{Eu}/\text{Fe}]$ , with Eu being dominated by r-process contributions, shows a strong scatter in low metallicity stars up to  $[\text{Fe}/\text{H}] < -2$ , arguing for a strongly reduced occurrence rate in comparison to core-collapse supernovae. The high neutron densities in ejected matter permit a violent r-process, encountering fission cycling of the heaviest nuclei in regions far from (nuclear) stability. Uncertainties in nuclear properties, like nuclear masses, beta-decay half-lives, fission barriers and fission fragment distributions affect the detailed abundance distributions. The modeling of the astrophysical events depends also on the hydrodynamic treatment, i.e. SPH vs. grid calculations, Newtonian vs. GR approaches, the occurrence of a neutrino wind after the merger and before the emergence of a black hole, and finally the properties of black hole accretion disks. We will discuss the effect of both (nuclear and modelling) uncertainties and conclude that binary compact mergers are probably a or the dominant site of the production of r-process nuclei in our Galaxy. A small caveat exists with respect to explaining the behavior of  $[\text{Eu}/\text{Fe}]$  at lowest metallicities and the question whether neutron star mergers can already contribute at such early times in galactic evolution.

## Contents

1. INTRODUCTION .....	3
2. OBSERVATIONAL EVIDENCE FOR <i>r</i> -PROCESS NUCLEOSYNTHESIS .....	4
2.1. Solar <i>r</i> -Process Abundances and Patterns in Low-Metallicity Stars.....	4
2.2. Early Galactic Evolution .....	4
2.3. Short Duration Gamma-Ray Bursts and Macronovae (Kilonovae).....	6
2.4. Recent Radioactive Additions to the Solar System.....	7
3. CONDITIONS FOR MAKING THE HEAVIEST ELEMENTS .....	8
3.1. Explosive Burning and Charged-Particle Freeze-Out .....	8
3.2. Neutron Captures in the <i>r</i> -Process .....	11
3.3. The Influence of Nuclear Properties .....	13
4. <i>r</i> -PROCESS IN COMPACT BINARY MERGERS .....	14
4.1. Dynamical Ejecta .....	14
4.2. Neutrino Winds and the Effect of Neutrino Spectra .....	14
4.3. Black Hole Accretion Disks .....	17
5. A NEED FOR AN <i>r</i> -PROCESS CONTRIBUTION FROM MASSIVE SINGLE STARS? .....	18
6. CONCLUSIONS .....	20

## 1. INTRODUCTION

Neutron stars, postulated shortly after the discovery of the neutron, were predicted as the final fate of massive stars, ending in supernova events (1). Their existence was proven in the 1960's after the first observations of pulsars (2). We have by now an extensive knowledge of the distribution of neutron star masses and the underlying equation of state, (e.g. 3, 4, 5), with the most precise determinations existing for binary systems. Shortly after the discovery of the binary pulsar (6), with an energy loss in agreement with General Relativity, it was found that this system would merge in  $10^8$  years. This led to the prediction that neutron star or neutron star - black hole mergers would eject *r*-process nuclei (7, 8, 9), followed up by a first detailed analysis of possible abundance distributions (10). Later predictions included that such mergers would be accompanied by neutrino bursts and gamma-ray bursts (11). The very first and later more precise estimates of the mass ejection from neutron star mergers in Newtonian approximation followed (12, 13, 14, 15), together with the very first detailed nucleosynthesis predictions (16).

More recently, extensive investigations have been undertaken with respect to nucleosynthesis predictions (17, 18, 19, 20, 21, 22, 23, 24, 25, 26, 27, 28, 29, 30, 31, 32, 33, 34, 35, 36, 37), with new approaches going beyond a Newtonian treatment, via conformally flat to fully relativistic treatments (e.g. 38, 39, 40, 22, 24, 26, 41, 42), including also the role of magnetic fields (43). Modern simulations do not only consider the composition of the dynamical ejecta, but also a neutrino wind composition (along the poles), where matter is ejected from the combined (initially rotationally stabilized) hot neutron star (e.g. 44, 20, 29, 31, 26, 41, 42, 45, 37), up to the point of black hole formation (46), if the maximum neutron stars mass is exceeded, and afterwards ejection of matter takes place from (viscous) black hole accretion disks. The outflow of black hole accretion disks has been investigated in detail in a number of studies, (e.g. 47, 48, 49, 27, 50, 35, 51) and the effect of neutrino conversion via matter-neutrino resonances has been analyzed with respect to a possible impact on nucleosynthesis (52, 53, 54, 55, 56). For a good overview of all these com-

ponents, including jet formation and ejection see (57). In parallel to neutron star mergers also neutron star - black hole mergers have been investigated (e.g. 58, 20, 59, 60, 61, 62, 63)

Such nucleosynthesis predictions have been extensively tested with respect to nuclear uncertainties due to masses far from stability, beta decays, fission barriers, and fission fragment distributions (e.g. 23, 28, 30, 32, 64, 51, 65). The effect of the nuclear equation of state was investigated as well (e.g. 39, 40, 22, 66, 27, 41, 67).

There exists extensive literature relating these events to short duration Gamma-Ray Bursts and/or macronovae/kilonovae as electromagnetic counterparts (for recent literature see e.g. 68, 69, 70, 71, 72, 25, 46, 73, 74, 75, 76, 63, 77). However, this issue was the central feature of last year's review by Fernandez & Metzger (78), and we refer here to that article. Although these objects are also of major importance as strong sources for gravitational wave emission (79), underpinning the importance of multi-messenger observations, we will essentially focus in the present review on the ejected nucleosynthesis composition. The nucleosynthesis is constrained by solar r-process abundances and whether they can be reproduced by compact object mergers, by observations of low metallicity stars which are affected by the occurrence frequency as a function of time during galactic evolution, and finally by information from individual events which relate to the observed light curve and spectra (here the nucleosynthetic composition connects via its effect on opacities to the electrodynamic signal). This review covers observational constraints in section 2, the required thermodynamic conditions and neutron-richness of the ejecta in section 3, and a detailed discussion of nucleosynthesis results from compact object mergers in section 4. Finally, in section 5 we come back to issues in galactic evolution and whether compact binary mergers can match observations in the early Galaxy, before presenting conclusions in section 6.

## 2. OBSERVATIONAL EVIDENCE FOR *r*-PROCESS NUCLEOSYNTHESIS

### 2.1. Solar *r*-Process Abundances and Patterns in Low-Metallicity Stars

One interesting aspect to be tested relates to the question whether mergers lead to a quite robust *r*-process environment, which each time produces the heavy *r*-elements (at least those with  $A \geq 130$ ) in proportions similar to solar (see Fig.1 and 81, 82). On the other hand there exist variations in the contribution of lighter elements with  $Z \leq 50$  (83). Could this be due to variations in the production site or require different production sites? A fraction of old metal-poor halo stars shows a large variety of abundance signatures, including also *r*-elements like Eu (see e.g. 84, 85, 86). Possibly this is indicating a different weaker neutron-capture source, maybe a fraction of regular supernovae (87, 88)? Finally it should also be noted, that not in all low-metallicity star observations Th and U show up in solar proportions (or with appropriate abundances due to their decay since production). Since their initial discovery (89), a number of such abundance patterns have been observed, up to now all in extremely metal-poor stars. This could indicate changes in the *r*-process strength for the same *r*-process sites.

### 2.2. Early Galactic Evolution

As mixing of ejecta into the interstellar medium is not instantaneous, there will be local inhomogeneities after individual nucleosynthesis events. Mixing occurs (a) via the plowing of a Sedov-Taylor blast wave through interstellar matter until the (kinetic) explosion energy is used up, working against the ram pressure of the surrounding medium. For a standard

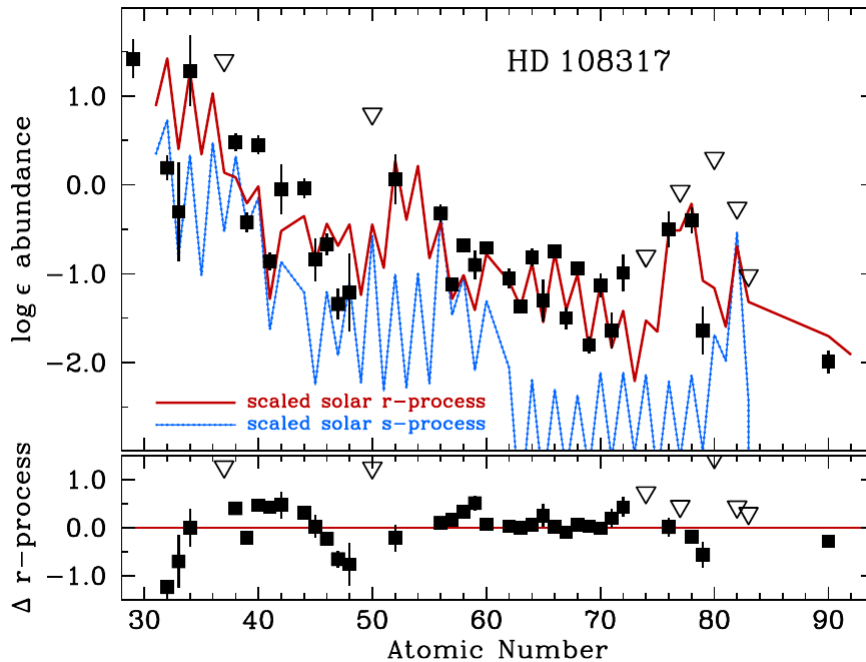


**Figure 1**

Shown are the observed abundances of typical low metallicity stars which unveil a clear r-process (and not an s-process) pattern, exactly as found in the solar system, at least for elements with  $Z \geq 40$  (80).

explosion energy of  $E = 10^{51}$  erg (a unit known as 1 Bethe, or 1 foe, an acronym based on 10 to the fifty-one ergs) and typical densities of the interstellar medium, this results in mixing with about a few times  $10^4 M_{\odot}$ . (b) There will be mixing via other more macroscopic phenomena, like e.g. turbulent mixing and/or spiral arm movements with time scales on the order of  $10^8$  y, for turbulent mixing being possibly as low as a few  $10^7$  y? While the latter effects can smooth spatial abundance gradients, the first one will keep the individual composition of a specific explosive event until many other events from different stellar sources/explosions pollute the interstellar medium in the same vicinity. This causes an integrated average of ejecta compositions. Thus, while we expect an average value of e.g. [Eu/Fe] to occur in late galactic evolution, rare events will lead to large variations at low metallicities, depending on whether or not a rare nearby strong r-process source polluted the environment.

Neutron star mergers have high predicted ejecta masses of the order of a few times  $10^{-3}$  to  $10^{-2} M_{\odot}$  of overall r-process matter in dynamical ejecta, and are rare in comparison to regular core-collapse supernovae (CCSNe) with a frequency being smaller by a factor of 100 to 1000 (93, 94). Such event rates are also consistent with population synthesis studies (95) and with (inhomogeneous) chemical evolution calculations (96, 62, 97, 98, 99, 100, 101, 102). The latter can follow local variations of abundances due the specific contributions by individual explosions. The scatter of r-process elements (e.g. Eu) compared to Fe at low metallicities covers more than two orders of magnitude (see Fig.2) and indicates production

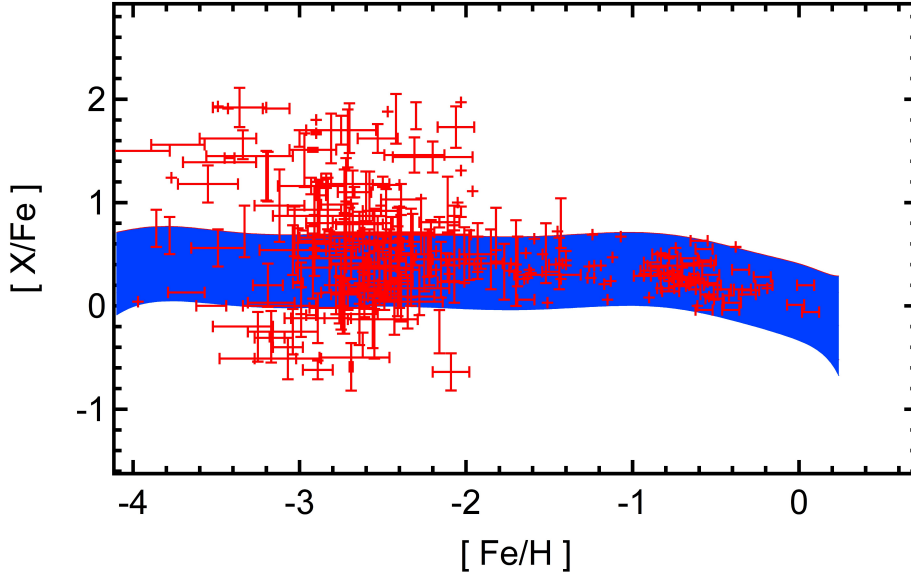


**Figure 2**

Ratios of  $[Mg/Fe]$  (blue uncertainty range, indicating 95% of observations) and  $[Eu/Fe]$  (individual stellar observations shown as red error bars) as a function of "metallicity"  $[Fe/H]$  for stars in our Galaxy, as displayed in (90) and taken from a database (91, 92).  $[X/Y]$  stands for  $\log_{10} [(X/Y)/(X/Y)_{\odot}]$ , i.e.  $[Mg/Fe]=0$  or  $[Fe/H]=0$  for solar ratios, -1 for 1/10 of solar etc.. Mg shows a relatively flat behavior up to  $[Fe/H] \leq -1$ , similar to other alpha elements like O, Mg, Si, S, Ar, Ca, Ti, turning down to solar values at  $[Fe/H]=0$ . This is explained by the early contributions of core-collapse supernovae before type Ia supernovae set in. The real scatter is probably smaller than indicated by the blue region, as this is a collection of many observations from different telescopes, different observers and different analysis techniques. To the contrary, the scatter of  $[Eu/Fe]$  is larger than two orders of magnitude at low metallicities, indicating production sites with a low event rate, and thus taking longer to arrive at average values only in the interval  $-2 \leq [Fe/H] \leq -1$ . Such average values are seen for alpha-elements (with core-collapse supernova origin) already in the range  $-4 \leq [Fe/H] \leq -3$

sites with negligible Fe production (103) and a low event rate combined with high ejecta masses in order to explain solar abundances. This causes the effect that for  $[Eu/Fe]$  the approach to an average ratio occurs only in the interval  $-2 \leq [Fe/H] \leq -1$ . It is shifted in comparison to the behavior of  $[Mg/Fe]$ , due to the much higher CCSNe rate. The latter permits a much earlier approach to an average ratio in the metallicity range  $[Fe/H] = -3$  to  $-4$ .

Dwarf galaxies, and especially ultra-faint dwarf galaxies, are polluted only by a few (104, 105, 106, 107) or in extreme cases only one single nucleosynthesis event, as e.g. seen in Reticulum II (108, 109). These observations, especially the latter, require events with high r-process ejecta masses, consistent with the above conclusions from low metallicity stars in the Milky Way. The Milky Way might evolve from an assembly of initially individual dwarf galaxies where the star formation efficiency and rate can vary in these early components, before the present galaxy emerges (110, 101, 111).

### 2.3. Short Duration Gamma-Ray Bursts and Macronovae (Kilonovae)

While in the previous subsection we discussed overall constraints, i.e. how to reproduce the solar r-process abundance pattern, indications for individual events are harder to obtain.

Low metallicity stars can serve here to some extent, as they might only have been polluted by one nucleosynthesis event. A clearer constraint is based on direct observations of a single event, in order to test whether theoretical predictions for an r-process are underpinned by observational proofs for these objects. Neutron star mergers have been identified with short duration gamma-ray bursts or macronovae via light curves and spectra of electromagnetic counterparts. These are not yet proofs for a detailed abundance pattern, but the existing observations can only be understood utilizing opacities of (very) heavy elements (e.g. 112, 69, 113, 72, 114, 74, 115, 78, 63, 77). The radioactive energy emitted from heavy unstable nuclear species, together with its thermalization efficiency, sets the luminosity budget and is therefore crucial for predicting macronova light curves. In modeling the macronova accompanying gamma-ray burst 130603B, estimates for the mass ejection could be made (76) in that event. This work also showed that late time macronova light curves can be significantly impacted by alpha-decay from translead isotopes. The latter could actually be a diagnostic test for more detailed ejecta abundances. We want to keep this discussion brief and refer the reader to last year's Annual Review article by Fernandez & Metzger on electromagnetic signatures of compact binary mergers, which discusses this topic in extended detail (78). The message to take home is that only with opacities of very heavy elements the light curves and spectra of these events are explainable, i.e. short durations GRBs produce these heavy elements in sizable amounts. While the observations integrate over many (also radioactive) elements, a detailed abundance pattern can not be determined, but there is hope to identify specific features with further investigations (76).

#### 2.4. Recent Radioactive Additions to the Solar System

While the above discussion points to rare strong r-process events in the early galaxy, there exist other observations, suggesting the same in recent history. Long-lived radioactive species can act as witness of recent additions to the solar system, dependent on their half-lives. For a review on the signature of radioactive isotopes alive in the early solar system see e.g. (116). Two specific isotopes have been utilized in recent years to measure such activities in deep sea sediments. One of them,  $^{60}\text{Fe}$ , has a half-life of  $2.6 \times 10^6$  y and can indicate recent additions from events occurring up to several million years ago.  $^{60}\text{Fe}$  is produced during the evolution and explosion of massive stars (leading to supernovae) (117, 118). It is found in deep-sea sediments which incorporated stellar debris from a nearby explosion about two million years ago (119, 120, 121, 122). Such a contribution is consistent with a supernova origin and related occurrence frequencies, witnessing the last nearby event. Another isotope utilized,  $^{244}\text{Pu}$ , has a half-life of  $8.1 \times 10^7$  y and would lead to a collection of quite a number of such supernova events. If the strong r-process would take place in every core-collapse supernova from massive stars, about  $10^{-4}$ - $10^{-5}$   $M_{\odot}$  of r-process matter would need to be ejected per event in order to explain the present day solar abundances. The recent  $^{244}\text{Pu}$  detection (123) is lower than expected from such predictions by two orders of magnitude, suggesting that actinide nucleosynthesis is very rare (permitting substantial decay since the last nearby event) and that supernovae did not contribute significantly to it in the solar neighborhood for the past few hundred million years. Thus, in addition to the inherent problems of (regular) core collapse supernova models to provide conditions required for a strong r-process - also producing the actinides - these observational constraints from nearby events also challenge regular CCSNe as source of main r-process contributions. A recent careful study of the origin of the strong r-process with continuous accretion of interstellar

dust grains into the inner solar system (34) concluded that the experimental findings (123) are in agreement with an r-process origin from a rare event like neutron star mergers. This explains the  $^{244}\text{Pu}$  existing initially in the very early solar system as well as the low level of more recent additions witnessed in deep-sea sediments over the past few hundred million years.

### 3. CONDITIONS FOR MAKING THE HEAVIEST ELEMENTS

Many sites for the r-process have been suggested in the past, from regular CCSNe, via neutrino-induced processes in outer shells of massive stars, ejecta from compact binary mergers, up to a special class of core collapse supernovae (MHD-jet supernovae) with fast rotation, high magnetic fields and neutron-rich jet ejecta along the poles. In any of these cases, the production of r-process nuclei occurs in a two stage process, defined by initial explosive burning at high temperatures until charged-particle freeze-out during the expansion with a high neutron/seed ratio. This is followed by the rapid capture of neutrons on these seed nuclei, producing the heaviest nuclei.

#### 3.1. Explosive Burning and Charged-Particle Freeze-Out

In the first stage matter experiences explosive burning at high temperatures and is heated to conditions which permit a so-called nuclear-statistical equilibrium (NSE), which indicates a full chemical equilibrium of all involved nuclear reactions. At density  $\rho$  and temperature  $T$  nucleus  $i$  - with neutron number  $N_i$ , proton number  $Z_i$ , and mass number  $A_i = Z_i + N_i$  - is existing with the abundance  $Y_i$ , expressed in terms of the abundances of free neutrons  $Y_n$  and protons  $Y_p$

$$Y_i = G_i(\rho N_A)^{A_i-1} \frac{A_i^{3/2}}{2^{A_i}} \left( \frac{2\pi\hbar^2}{m_u k_b T} \right)^{3/2(A_i-1)} \exp(B_i/k_b T) Y_n^{N_i} Y_p^{Z_i}, \quad (1)$$

where  $G_i$  is the partition function of nucleus  $i$ ,  $N_A$  is Avogadro's number,  $m_u$  the nuclear mass unit,  $k_b$  the Boltzmann constant, and  $B_i$  the nuclear binding energy of the nucleus. Beta-decays, electron captures, and neutrino interaction, change the overall proton to nucleon ratio  $Y_e = \sum Z_i Y_i / \sum A_i Y_i$  (the denominator is the sum of all mass fractions and therefore equal to unity) and occur on longer time scales than particle captures and photodisintegrations. They are not in equilibrium and have to be followed explicitly. Thus, as a function of time the NSE will follow the corresponding densities  $\rho(t)$ , temperatures  $T(t)$ , and  $Y_e(t)$ , leading to two equations based on total mass conservation and the existing  $Y_e$

$$\sum_i A_i Y_i = Y_n + Y_p + \sum_{i>n,p} (Z_i + N_i) Y_i(\rho, T, Y_n, Y_p) = 1 \quad (2)$$

$$\sum_i Z_i Y_i = Y_p + \sum_{i>p} Z_i Y_i(\rho, T, Y_n, Y_p) = Y_e. \quad (3)$$

In general, very high densities favor large nuclei, due to the high power of  $\rho^{A-1}$ , and very high temperatures favor light nuclei, due to  $(kT)^{-3/2(A-1)}$ . In the intermediate regime  $\exp(B_i/kT)$  favors tightly bound nuclei with the highest binding energies in the mass range



$A = 50 - 60$  of the Fe-group, but depending on the given  $Y_e$ . The width of the composition distribution is determined by the temperature. Thus, in this first stage of the scenario discussed here, high temperatures cause the (photo-)disintegration of nuclei into neutrons, protons, and alpha-particles, due to the energy distribution of the black body photon gas. During the subsequent cooling and expansion of matter, a build-up of heavier nuclei sets in, still being governed by the trend of keeping matter in NSE. However, the build-up of nuclei beyond He is hampered by the need of reaction sequences involving highly unstable  ${}^8\text{Be}$  (e.g.  $\alpha + \alpha + \alpha \rightarrow {}^{12}\text{C}$  or  $\alpha + \alpha + n \rightarrow {}^9\text{Be}$ ) which are strongly dependent on the density of matter. The first part of these reaction sequences involves a chemical equilibrium for  $\alpha + \alpha \leftrightarrow {}^8\text{Be}$  which is strongly shifted to the left side of the reaction equation, due to the half life of  ${}^8\text{Be}$  ( $\tau_{1/2} = 6.7 \times 10^{-17}\text{s}$ ). Reasonable amounts of  ${}^8\text{Be}$ , which permit the second stage of these reactions via an alpha or neutron-capture, can only be built-up for high densities. The reaction rates for the combined reactions have a quadratic dependence on density in comparison to a linear density dependence in regular fusion reactions. Therefore, for low densities the NSE cannot be kept and after further cooling and freeze-out of charged-particle reactions an overabundance of alpha particles (helium) remains, permitting only a (much) smaller fraction of heavier elements to be formed than in an NSE for the intermediate regime (determined by binding energies of nuclei). This result is also called an alpha-rich freeze-out (of charged-particle reactions) and leads to the fact that (a) the abundance of nuclei heavier than He is (strongly) reduced in comparison to their NSE abundances, and (b) the abundance maximum of the (fewer) heavy nuclei is shifted (via final alpha captures) to heavier nuclei in comparison to an NSE. While this maximum would normally be around Fe and Ni (the highest binding energies) with  $A=50-60$ , it can be shifted up to  $A$  about 90.

In hot environments the total entropy is dominated by the black-body photon gas (radiation) and proportional to  $T^3/\rho$  (124, 125), i.e. the combination of high temperatures and low densities leads to high entropies. Thus, high entropies cause an alpha-rich freeze-out, and - dependent on the entropy - only small amounts of Fe-group elements are produced, essentially all matter which passed the bottle neck beyond He. This result is shown in Fig.3a.

The calculation for Fig.3a, performed with an expansion time scale equivalent to a free-fall for those conditions and a  $Y_e = 0.45$ , shows how with increasing entropies the alpha mass-fraction ( $X_\alpha = 4Y_\alpha$ ) is approaching unity and the amount of heavier elements (which would provide the seed nuclei for a later r-process) is going to zero. This is similar to the big bang, where extremely high entropies permit essentially only elements up to He, and tiny amounts of Li. Opposite to the big bang, which is proton-rich, the conditions chosen here ( $Y_e = 0.45$ ) are slightly neutron-rich, leading at high entropies predominantly to He and free neutrons. The small amount of heavier nuclei after this charged-particle freeze-out (in the mass range of  $A=50-100$ ), depending on the entropy or alpha-richness of the freeze-out, can then act as seed nuclei for capture of the free neutrons. As prerequisite for an r-process, producing nuclei as heavy as the actinides and starting from  $A=50-100$  nuclei, a neutron/seed ratio of about 150 is required. This ratio is plotted in the form of a contour plot and as a function of entropy and  $Y_e$  in Fig.3b, based on (127).

A different behavior occurs for lower entropies, i.e. the expansions of relatively cold and/or high density matter, as it would exist in ejected neutron star matter. At such low entropies the contour lines for constant n/seed ratios of Fig.3b will bend over and become flat, with the resulting neutron/seed ratio being essentially only a function of  $Y_e$ . In order to obtain then an n/seed ratio of 150, a  $Y_e$  of the order 0.1 is required.

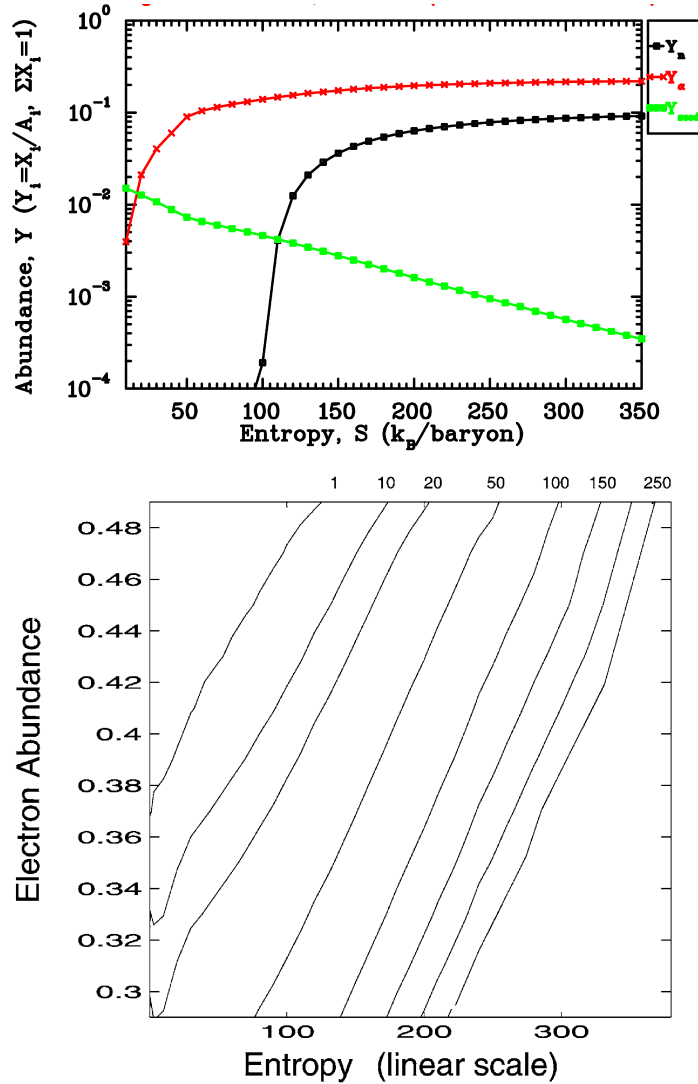


**Figure 3**

Top: Abundances of neutrons  $Y_n$ ,  ${}^4\text{He}$  (alpha-particles)  $Y_\alpha$ , and so-called seed nuclei  $Y_{seed}$  (in the mass range  $50 \leq A \leq 100$ ), resulting after the charged particle freeze-out of explosive burning, as a function of entropy in the explosively expanding plasma, based on results by (126). It can be realized that the ratio of neutrons to seed nuclei ( $n/seed = Y_n/Y_{seed}$ ) increases with entropy. The number of neutrons per seed nucleus determines whether the heaviest elements (actinides) can be produced in a strong r-process, requiring  $A_{seed} + n/seed \geq 230$ . Bottom:  $n/seed$  ratios (shown as contour lines) resulting in expanding hot plasmas from explosive burning as a function of the electron abundance  $Y_e$  and the entropy (measured in  $k_b$  per baryon). A strong r-process, producing the actinides with  $n/seed$  of 150, requires for moderate  $Y_e$ 's, of about 0.45, entropies beyond 250 (127).

### 3.2. Neutron Captures in the r-Process

Once a freeze-out of charged-particle reactions and full chemical equilibrium (NSE) occurred, resulting in a high neutron/seed ratio, the actual r-process - powered solely by the rapid capture of neutrons - can start, at temperatures below  $3 \times 10^9$  K and all nuclear reactions have to be followed in full detail. This leads to three types of terms in reaction network equations. The nuclear abundances  $Y_i$  enter in this set of equations and their time derivative can be written in the form

$$\frac{dY_i}{dt} = \sum_j P_j^i \lambda_j Y_j + \sum_{j,k} P_{j,k}^i \rho N_A \langle j, k \rangle Y_j Y_k + \sum_{j,k,l} P_{j,k,l}^i \rho^2 N_A^2 \langle j, k, l \rangle Y_j Y_k Y_l. \quad (4)$$

One has to sum over all reaction partners given by the different summation indices. The  $P$ 's include an integer (positive or negative) factor  $N^i$ , describing whether (and how often) nucleus  $i$  is created or destroyed in this reaction, but also correction factors avoiding multiple counting in case two or three identical reaction partners are involved. The  $\lambda$ 's stand for decay rates (including decays, photodisintegrations, electron captures and neutrino-induced reactions),  $\langle j, k \rangle$  denotes the thermal average for the product of reaction cross section  $\sigma$  and relative velocity  $v$  of reactions between nuclei  $j$  and  $k$ , while  $\langle j, k, l \rangle$  includes a similar expression for three-body reactions (128). For a survey of computational methods to solve nuclear networks see (129, 130). The abundances  $Y_i$  are related to number densities  $n_i = \rho N_A Y_i$  and mass fractions of the corresponding nuclei via  $X_i = A_i Y_i$ . Data repositories of experimental and theoretical reaction rates required as input for equation 4 can be found e.g. on the following websites <https://groups.nsl.msu.edu/jina/reaclib/db/>, <https://nuastro.org/reaclib.html>, and <http://www.kadonis.org/>, <http://www.astro.ulb.ac.be/pmwiki/Brusslib/HomePage>. A more detailed discussion of modeling nucleosynthesis processes is given in (117).

As charged-particle reactions are frozen at about  $3 \times 10^9$  K, the only connection between isotopic chains is given by beta-decays (unless fission will set in, repopulating lighter nuclei from fission fragments). High neutron densities make the timescales for neutron capture much faster than those for beta-decay and can produce nuclei with neutron separation energies  $S_n$  of 2 MeV and less. This is the energy gained (Q-value) when capturing a neutron on nucleus  $A - 1$  and or the photon energy required to release a neutron from nucleus  $A$  via photo-disintegration. At the neutron drip-line  $S_n$  goes down to 0, i.e. for the high neutron densities of such an r-process it proceeds close to the neutron drip-line. For temperatures around  $10^9$  K,  $(\gamma, n)$  photodisintegrations can still be very active for such small reaction  $S_n$ -values, as only temperatures related to about  $30kT \geq S_n$  are required for these reverse reactions to dominate. With both reaction directions being faster than process timescales (and beta-decays) a chemical equilibrium can set in between neutron captures and photodisintegrations. In such a case, a complete chemical or nuclear statistical equilibrium (NSE) - discussed in the beginning of this subsection - splits into many (quasi-) equilibrium clusters, representing each an isotopic chain of heavy nuclei. The abundance distribution in each isotopic chain follows the ratio of two neighboring isotopes

$$\frac{Y(Z, A+1)}{Y(Z, A)} = n_n \frac{G(Z, A+1)}{2G(Z, A)} \left[ \frac{A+1}{A} \right]^{3/2} \left[ \frac{2\pi\hbar^2}{m_u k_b T} \right]^{3/2} \exp(S_n(A+1)/k_b T). \quad (5)$$

with partition functions  $G$  describing the thermal population of excited states, the nuclear-mass unit  $m_u$ , and the neutron-separation (or binding) energy of nucleus  $(Z, A+1)$ ,

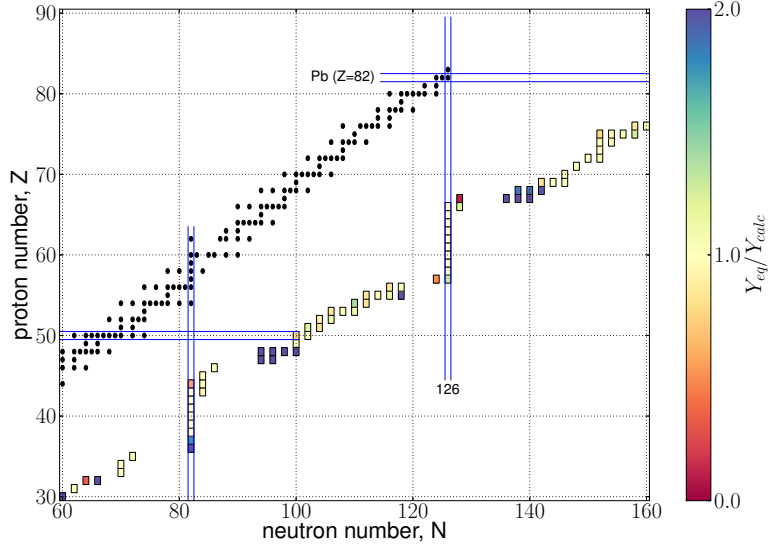


**Figure 4**

Shown is (a) the line of stability (black squares) and (b) the r-process path, resulting here from a neutron star merger environment which will be discussed further below (30). The position of the path follows from a chemical equilibrium between neutron captures and photo-disintegrations in each isotopic chain ( $(n, \gamma) - (\gamma, n)$  equilibrium), determined by the neutron number density and temperature. However, the calculation was performed with a complete nuclear network containing more than 3000 nuclei. The colors along the path indicate how well the full network calculation follow such an  $(n, \gamma) - (\gamma, n)$  equilibrium. It can be seen that such full calculations agree with this equilibrium approach within a factor of 2 along the r-process path, which continues to the heaviest nuclei. Only in the final phase of the process, when neutron number densities and temperatures decline, such an equilibrium freezes out and some final changes of the abundance pattern can occur due to still continuing neutron captures.

$S_n(A+1)$ , being the neutron-capture  $Q$ -value of nucleus  $(Z, A)$ . The abundance ratios are dependent only on  $n_n = \rho N_A Y_n$ ,  $T$  and  $S_n$ .  $S_n$  introduces the dependence on nuclear masses, i.e. a nuclear-mass model for these very neutron-rich unstable nuclei. Under the assumption of an  $(n, \gamma) \rightleftharpoons (\gamma, n)$  equilibrium, no detailed knowledge of neutron-capture cross sections is needed.

One fact which can be easily deduced, given that  $Y(A+1)/Y(A)$  is first rising with increasing distance from stability, close to 1 at the abundance maximum of the isotopic chain, and finally decreasing, is that the abundance maxima in each isotopic chain are only determined by the neutron number density  $n_n$  and the temperature  $T$ . Approximating  $Y(Z, A+1)/Y(Z, A) \simeq 1$  at the maximum and keeping all other quantities constant, the neutron-separation energy  $S_n$  has to be the same for the abundance maxima in all isotopic chains (see Fig.4). It should be said at this point that all present nucleosynthesis calculation are obtained from full solutions of extended reaction networks determined by the set of equations 4. However, the use of the approximations 1, 3 and 5 can act as tests whether such equilibria exist and aids understanding the numerical results. Fig.4 displays exactly such a test for the conditions in neutron star mergers (30).

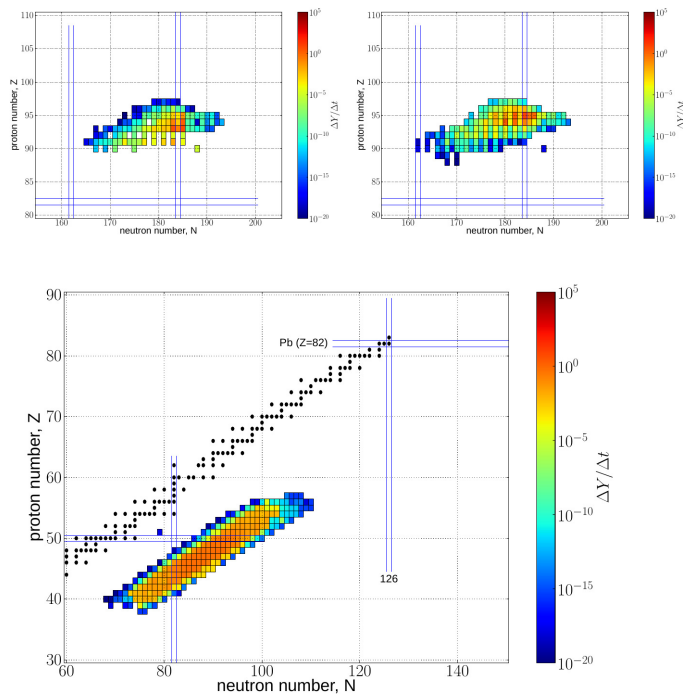


**Figure 5**

Shown are (color-coded) time derivatives of nuclear abundances  $Y$  during an r-process simulation (30), due to (a) the destruction via neutron-induced and beta-delayed fission (131) and (b) the production of fission fragments (132). The latter are produced in a broad distribution, ranging in mass numbers  $A$  from 115 to 155.

### 3.3. The Influence of Nuclear Properties

Fig.4 shows a contour line of  $S_n \simeq 2$  MeV for the FRDM mass model (133). In addition, it displays the line of stability. As the speed along the r-process path is determined by beta-decays, and they are longest closer to stability, abundance maxima will occur at the top end of the kinks in the r-process path at neutron shell closures  $N = 50, 82, 126$ . This causes abundance maxima at the appropriate mass numbers  $A$  after decay back to stability at the end of the process, which correspond to smaller mass numbers  $A$  than those for stable nuclei with neutron shell closures. In environments with sufficiently high neutron densities, the r-process continues to extremely heavy nuclei and finally encounters the neutron shell closure  $N = 184$ , where fission plays a dominant role. Fig.5 (based also on simulations by 30) shows the regions of the nuclear chart where fission dominates and where the fission fragments are located.

After having discussed here the general working of and the nuclear input for an r-process, the following chapter is related to apply this to neutron star merger environments. Independent of the encountered conditions, the influence of nuclear uncertainties should be analyzed, and how they affect the obtained results. Recent tests with respect to mass models, beta-decay half-lives, and fission fragment distributions have been performed by (64, 30, 23, 32, 51) utilizing a variety of mass models, beta decay, and fission properties

(133, 134, 135, 136, 137, 138, 139, 17, 131, 140, 132, 23) as well as analyzing the effect of neutrinos (see e.g. 29, 28, 31) were the most advanced treatment of neutrino interactions in matter with medium corrections are given by (141, 142). Finally, also tests for neutrino flavor conversion via matter-neutrino resonances have been performed (e.g. 55, 56).

## 4. r-PROCESS IN COMPACT BINARY MERGERS

A brief overview with regard to the history of neutron star-black hole or binary neutron star mergers, especially their role with respect to their nucleosynthesis contributions, has been given in section 1. Here we want to discuss the main results obtained in recent research (e.g. 18, 19, 20, 21, 22, 23, 24, 25, 26, 28, 29, 27, 30, 31, 32, 41, 33, 34, 35, 42, 67, 36, 51, 37). These include simulations which do not only consider the composition of the dynamical ejecta, but also a neutrino wind composition (along the poles), where matter is ejected from the combined (initially rotationally stabilized) hot neutron star up to the point of black hole formation, and afterwards the ejection of matter from (viscous) black hole accretion disks. In the following we discuss these aspects in separate subsections.

### 4.1. Dynamical Ejecta

One of the aspects of earlier investigations, studying only the dynamical ejecta, i.e. matter "thrown out" dynamically after the merger of two compact objects with very low  $Y_e$ , was that abundances below the second r-process peak (at  $A=130$ ) would only result from fission products. Thus, lighter r-process elements beyond the Fe-group have already experienced neutron capture and are depleted in the final results. In addition, especially for Newtonian calculations, material had the tendency to be possibly too neutron-rich. This led to large amounts of very heavy nuclei prone to fission, remaining close to the end of the simulations. While initial conditions during the working of the r-process seem perfect to reproduce the second and third r-process peak and their positions (see the location of the kinks in the contour line of constant neutron separation energy in Fig.4), during the final phase the fission of the heaviest nuclei produces large amounts of neutrons. If this happens during/after the freeze-out from  $(n, \gamma)$ -  $(\gamma, n)$  equilibrium, these neutrons can modify the overall abundance pattern inherited from the earlier equilibrium, especially shifting the third r-process peak. A number of tests, based on latest knowledge of nuclear physics far from stability, have been performed and can improve the overall abundance pattern. This relates to mass model properties like fission probabilities and fragment distributions (see Fig.6) as well as beta-decay half-lives (139, 140), which speed up the production of the heaviest nuclei and lead to the fact that the final phase of fission sets in earlier with respect to the freeze-out and the smaller release of late neutrons has less effect on the pattern of the third r-process peak (see Fig.6ab and 30).

### 4.2. Neutrino Winds and the Effect of Neutrino Spectra

Another aspect is that also a "neutrino-wind" (similar to that in CCSNe) from the hot, very massive combined object of the two neutron stars will contribute to the nucleosynthesis of these events after the dynamic ejecta discussed above. This hot central object, supported by high temperatures and rotation, will not collapse to a black hole immediately, and surrounding matter experiences the radiation of neutrinos and antineutrinos, changing the  $Y_e$  by the reactions

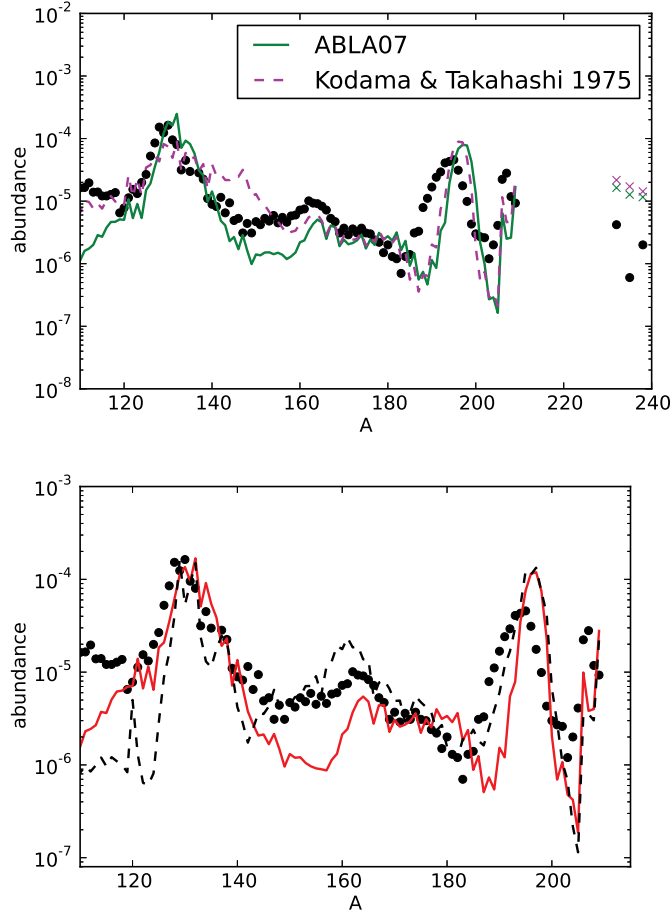


**Figure 6**

Top: Resulting  $r$ -process abundances (in comparison to solar values - black dots) from neutron star merger simulations (30), making use of beta-decay half-lives from (138) together with a relatively old (143) and a modern set (132) of fragment distributions of fissioning nuclei. However, in both cases a shift of the third  $r$ -process peak seems to occur in the final phases, driven by neutron capture of the released fission neutrons. Bottom: Same as above, but utilizing recent beta-decay half-life predictions (139) (dashed black line) in comparison to the older set (red line, identical to green line from top figure). Faster beta-decays for heavy nuclei, cause a speed-up of the  $r$ -process and deliver (also in the final phases) nuclei which are prone to fission at an earlier time. This way, the late release of fission neutrons occurs earlier, to a large extent before the freeze-out from  $(n, \gamma)$ - $(\gamma, n)$  equilibrium. Therefore, final neutron captures after freeze-out, which can distort this distribution, are strongly reduced. This can be seen when comparing top and bottom figure.



These reactions turn matter only neutron-rich if the average antineutrino energy  $\langle \epsilon_{\bar{\nu}_e} \rangle$  is

higher than the average neutrino energy  $\langle\epsilon_{\nu_e}\rangle$  by 4 times the neutron-proton mass difference  $\Delta$  for similar (electron) neutrino  $L_{\nu_e}$  and antineutrino  $L_{\bar{\nu}_e}$  luminosities. This was pointed out initially in (144), leading - when approaching equilibrium conditions for neutrino and antineutrino captures - to

$$Y_e = \left[ 1 + \frac{L_{\bar{\nu}_e}(\langle\epsilon_{\bar{\nu}_e}\rangle - 2\Delta + 1.2\Delta^2/\langle\epsilon_{\bar{\nu}_e}\rangle)}{L_{\nu_e}(\langle\epsilon_{\nu_e}\rangle + 2\Delta + 1.2\Delta^2/\langle\epsilon_{\nu_e}\rangle)} \right]^{-1} \quad (8)$$

For further details and in-medium corrections for neutrons and protons in comparison to their treatment as free particles see (141, 142). Thus, in most cases the energetically favorable first reaction wins, changing  $Y_e$  from the initial (neutron-rich) conditions towards values closer to  $Y_e = 0.5$ , which leads only to a weak r-process and produces matter below the second r-process peak. A first estimate of this outcome was presented in (25). More detailed results have been shown in (29, 31, 36, 45, 37), see e.g. Fig.7.

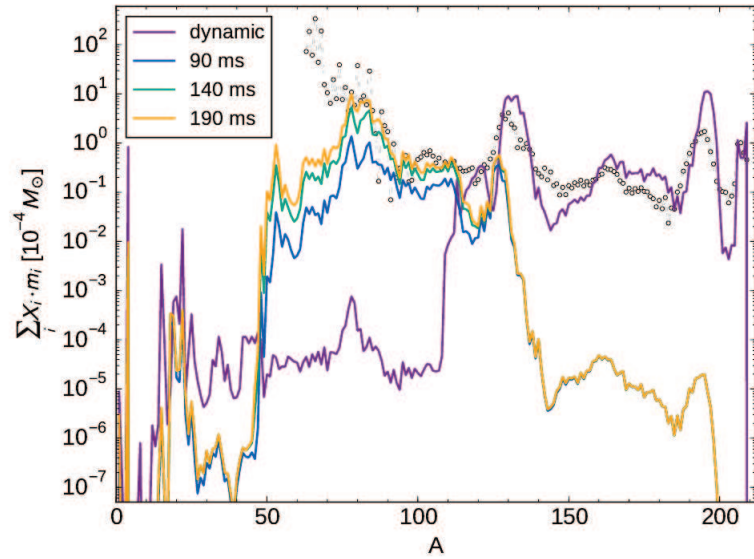


**Figure 7**

Neutrino wind contribution to neutron star merger ejecta, dependent on the delay time between the merger and BH formation (31). In comparison also the dynamic ejecta of (20) are shown. The neutrino wind, ejected dominantly in polar regions, contributes nuclei with  $A < 130$ , due to the effect of the neutrinos on  $Y_e$ .

There exists a related aspect, which also affects the dynamical ejecta. A number of simulations discussed above have been performed with Newtonian physics, i.e. non-relativistically. For neutron stars, and especially finally resulting black holes the role of general relativity is important and leads to deeper gravitational potentials plus higher temperatures experienced by the matter involved. This increases the importance of electron-positron pairs, positron captures on neutrons and also the effect of neutrino radiation even for the dynamical ejecta. In total this increases  $Y_e$  from 0.05 or less in pure neutron star matter to values around 0.1-0.15 (26, 28, 41, 42) for dynamical ejecta and to even higher values in the neutrino wind. As a result less fission cycling occurs, which produces less late emission of fission neutrons, and therefore avoids some of the deficiencies of the abundance



patterns discussed above with respect to Fig.6, also seen in the dynamic ejecta component of Fig.7.

Possible changes of  $Y_e$  can also be attained by the modification of neutrino and antineutrino spectra due to neutrino flavor conversion. There have been a number of tests to verify such neutrino conversions via matter-neutrino resonances (52, 53, 54, 55, 56). The more complicated geometry of a disk environment in comparison to CCSNe permits until presently only single-angle approximations which might limit the accuracy of present results. But the existing investigations clearly point to the potential that  $Y_e$ , and thus the resulting nucleosynthesis, can be affected.

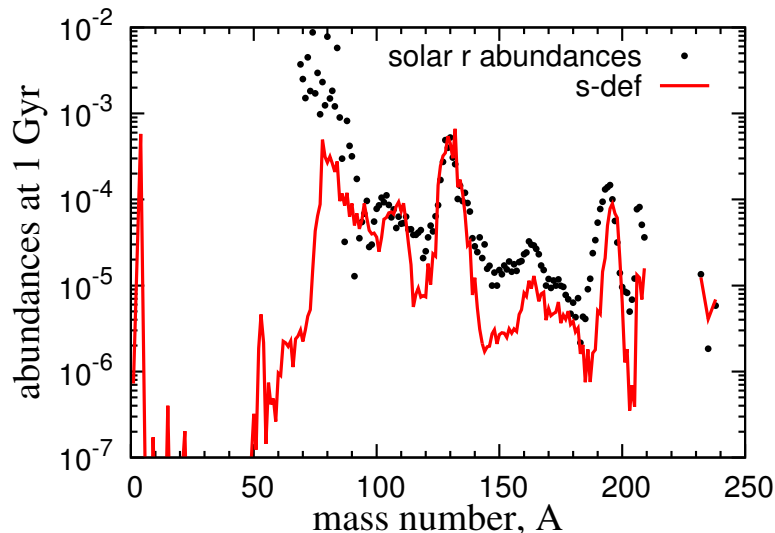


**Figure 8**

Resulting r-process abundances (in comparison to solar values - black dots) from black hole accretion disk simulations (51), making use of a black hole mass of  $3 M_{\odot}$ , a disk mass of  $0.03 M_{\odot}$ , an initial  $Y_e$  of 0.1, entropy per baryon of  $8k_b$ , an alpha parameter of the viscous disk of 0.03, and a vanishing black hole spin.

### 4.3. Black Hole Accretion Disks

After the stabilizing effect of rotation of the merged quite massive object fades, in most cases (being beyond the maximum mass of cold neutron stars) a central black hole will form. Such environments, resulting as the final fate of neutron star mergers, require investigations into disk winds from black hole accretion disks, which had initially been tested as sites of heavy element nucleosynthesis (47, 48, 49). Detailed simulations for these sites resulting from binary compact object mergers have been performed in recent years (27, 78, 35, 51), leading to predictions of comparable masses in dynamical ejecta and disk outflows (with a slight dominance of dynamical ejecta for neutron star mergers and the opposite effect for neutron star - black hole mergers (78)). Latest results for disk outflows (51) are displayed in Fig.8, which shows the integrated ejecta of all tracer particles. This underlines that outflows alone can produce a robust abundance pattern around the second r-process peak at  $A = 130$ , with a significant production of  $A \leq 130$  nuclei. Disk outflows also reach the third peak at  $A = 195$  in most of their simulations. The detailed results depend on the

disk viscosity, initial mass or entropy of the torus, the black hole spin, and (of course) the nuclear physics input. Especially the production of heavy ( $A=195$ ) nuclei is affected by the uncertainties of these disk properties. However, such a deficit can be easily counterbalanced by the dynamic ejecta, as the total nucleosynthesis of the merger includes the components of the dynamic ejecta, the neutrino wind, and the BH accretion disk.

## 5. A NEED FOR AN r-PROCESS CONTRIBUTION FROM MASSIVE SINGLE STARS?

The previous sections showed that compact binary mergers can reproduce in all cases the heavy (if not most of the) solar r-process abundances, they can explain short duration GRBs and related macronova(kilonova) events, they are rare, consistent with low metallicity observations and deep sea sediments, and in combination of ejecta masses and occurrence frequency they can also explain the total amount of solar r-process matter (within the given uncertainties). There seems to be only one caveat. A binary neutron star merger requires two prior supernova events (producing the two neutron stars and e.g. Fe-ejecta) plus the gravitational wave inspiral leading to the merger. There is a time delay between the Fe-producing supernovae and r-process ejection which can shift the appearance of a typical r-process tracer like Eu to higher metallicities  $[\text{Fe}/\text{H}]$  (see Fig.9), as discussed in (96, 97, 100). Such results rely to some extent on the coalescence times (and their distribution) in binary systems, the local star formation rate, and the amount of mixing of the ejecta with the surrounding interstellar medium, (see also 33). The results shown in Fig.9 are based on mixing with the surrounding medium via a Sedov-Taylor blast wave, i.e. typically of the order  $5 \times 10^{-4} M_{\odot}$  and with varying coalescence times. The latter seems not to solve the problem to reproduce the  $[\text{Eu}/\text{Fe}]$  ratios in low metallicity stars.

However, there exist other galactic mixing events on varying timescales (like turbulent mixing) which could blur the picture. Relatively low resolutions in global galaxy evolution models with smooth particle hydrodynamics simulations (98, 99) can wash out the behavior of Fig.(9) at low metallicities, but a high resolution run in (98) recovers it (see their Fig.4). The history of the local star formation rate can differ, if the Galaxy formed from small substructures which merge at late times in galactic evolution (110, 101). Such aspects still need to be worked out. Alternatively a rare class of CCSNe, exploding earlier in galactic evolution with negligible time delay to star formation, could contribute at low metallicities with negligible time delay to star formation. Early suggestions that so-called electron-capture supernovae in the stellar mass range 8-10  $M_{\odot}$  (145, 146, 147, 148) would be able to produce a strong r-process were never confirmed, and they would also not correspond to rare events. However, other objects driven by strong magnetic fields and fast rotation (possibly about 1% or less of all core-collapse supernovae), leaving behind  $10^{15}$  Gauss neutron stars (magnetars), might play a significant role. Such magneto-rotational SNe show similar characteristics in the amount of r-process ejecta and possibly the occurrence frequency as neutron star mergers, but - because these objects result from massive single stars - they do not experience the delay of binary evolution (149, 150, 151, 152, 87, 153, 88). This might be interesting with respect to the subdivision of short duration GRBs in those with a delay and those following directly the star formation rate (73).

Such magneto-rotational SNe, being also rare events and prolific in r-process ejecta, could enter galactic evolution at lowest metallicities with a similar scatter as binary compact mergers. Existing observations show evidence for the occurrence of MHD-jet super-

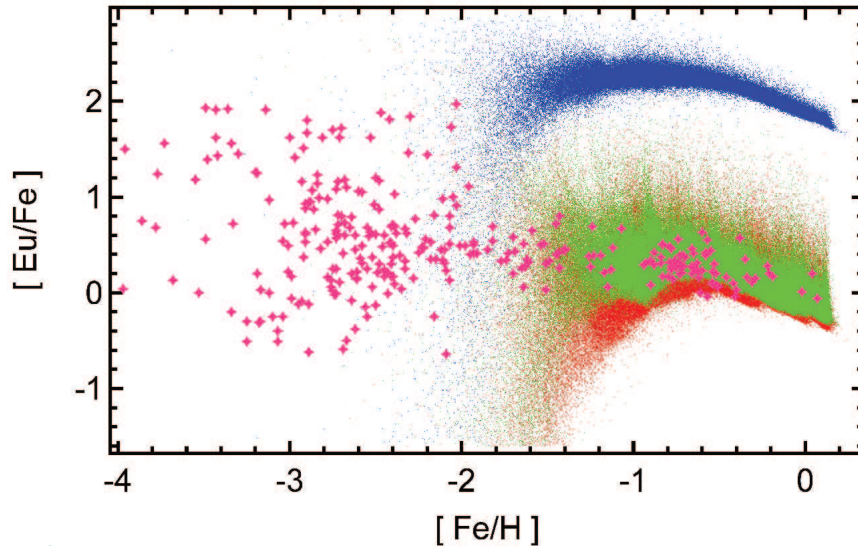


**Figure 9**

Influence of coalescence time scale and neutron star merger probability on Eu-abundances in galactic chemical evolution. Magenta stars represent observations. Red dots correspond to model star abundances as in (96). The coalescence time scale utilized is  $10^8$  years with a typical probability consistent with population synthesis (100). Green dots illustrate the effect on the abundances if the coalescence time scale is shorter (around  $10^6$  years). Blue dots show the abundance change if the probability of neutron star mergers is increased. Within this treatment of galactic chemical evolution, none of these options would permit a fit with observations of low metallicity stars in the metallicity range  $-4 \leq [\text{Fe}/\text{H}] \leq -2.5$ .

novae (magnetars 154). In inhomogeneous galactic evolution simulations without extended turbulent mixing a superposition of MHD-jet supernovae and neutron star mergers can match observations from lowest metallicities up to present. We should keep in mind that there exist uncertainties in mixing processes, star formation rates etc. which will affect the behavior at lowest metallicities. However, as shown in (87, 88), dependent on rotation frequency, magnetic fields, and the impact of neutrino heating in comparison to the strength of magnetic fields, the strength of the r-process can vary, while neutron star mergers seem to predict a robust and unchangeable abundance pattern. At low metallicities, there exist observations with a somewhat changing Eu/U ratio, indicating to which extent the production of actinides is robustly coupled to Eu. Few events with a regular r-process pattern but changing amounts of actinides are all seen at metallicities around  $[\text{Fe}/\text{H}] = -3$ . Thus, such variations, not expected from compact binary mergers might point to the effect of MHD supernovae at low metallicities. It is reasonable to expect that at that low metallicity MHD SNe are more frequent than in the present Galaxy. Low metallicity stars have smaller amounts of wind/mass and (therefore) angular momentum loss, providing more promising initial conditions at the onset of collapse for these events.

## 6. CONCLUSIONS

This review summarizes our present knowledge of r-process conditions in compact binary mergers, their ability to produce a solar abundance pattern, their role in galactic evolution and recent additions to the solar system, and finally also some open questions which still need to be solved or complemented by other sites:

1. It has been shown in extended sets of simulations that compact binary mergers are prolific sites of r-process nucleosynthesis, leading to about a few times  $10^{-3}$  to  $10^{-2}$   $M_{\odot}$  of ejected r-process matter in the dynamical ejecta and possibly a similar amount via black hole accretion disk wind (see Figure 4 in (78) and Figure 2 in (63)). When including all components - from dynamic ejecta over neutrino winds and final, viscous black hole accretions disks - they produce not only the heaviest r-process nuclei but also significant amounts of the standard solar r-process abundances for mass numbers with  $A < 130$ . The sizable production of r-process matter requires that these events are rare if they are responsible for reproducing all of galactic r-process material.
2. Radioactive tracers like  $^{244}\text{Pu}$  as well as  $^{60}\text{Fe}$  are found in deep sea sediments. The production of  $^{60}\text{Fe}$  in frequent events, related to regular CCSNe and/or electron capture supernovae, is supported by the latest contribution dating back about 2 million years. On the contrary, the amount of  $^{244}\text{Pu}$  found in these sediments is lower than expected by about a factor of 100, if a quasi-continuous production is assumed. This points to substantial decay since the last addition and to much rarer events.
3. Observations of lowest metallicity stars in our Galaxy and (ultra-faint) dwarf galaxies show substantial "pollution" by r-process elements, indicating a production site with a low event rate and consistent high amount of r-process ejecta in order to explain solar abundances. This is also underlined by the large scatter of  $\text{Eu}/\text{Fe}$  ( $\text{Eu}$  being an r-process element and  $\text{Fe}$  stemming from CCSNe at these low metallicities) seen in the earliest stars of the Galaxy, indicating that in a not yet well mixed interstellar medium the products of regular CCSNe and these rare events vary substantially.
4. We also know that neutron star mergers (or neutron-star black hole mergers) are related to short-duration gamma-ray bursts and electromagnetic counterparts (macronovae). The latter can only be explained if the opacity of ejected matter is dominated by heavy elements. Population synthesis supports that these events are very rare (probably about 1/100 of the CCSN frequency).
5. The major open question is whether products of the neutron star merger r-process can explain the observations of r-process elements seen already at metallicities of  $[\text{Fe}/\text{H}] \leq -3$ . As the supernovae which produce the neutron stars of a merger already lead to a substantial floor of  $\text{Fe}$ , i.e. enhance  $[\text{Fe}/\text{H}]$ , only substantial turbulent mixing of interstellar medium matter in the early Galaxy could reproduce these observations in galactic chemical evolution calculations.
6. There exist observational indications of  $10^{15}$  Gauss neutron stars. A rare class of CCSNe driven by a magneto-rotational mechanism could lead to such neutron stars with immense magnetic fields and produce r-process matter ejected in polar jets. However, predictions from stellar evolution about the distribution of magnetic fields and rotation rates before core collapse are needed in order to understand the initial conditions possibly leading to such events and the role of the magneto-rotational instability (MRI) during the collapse/explosion phase has to be investigated.
7. Such objects, very likely also with a low event rate of the order 1/100 of regular

CCSNe could possibly avoid the problems of the neutron star merger scenario at low metallicities, as they are related to massive single stars and do not experience any delay in comparison to regular CCSNe.

8. Independent of these points related to astrophysical observations and modelling complex astrophysical sites, the final test whether the detailed abundance pattern of heavy elements can be reproduced relies on a deep knowledge and understanding of nuclear properties which enter such calculations, from masses far from stability over weak interactions, determining beta-decay properties, electron/positron captures, and neutrino properties and interaction with matter, up to fission barriers and fission fragment distributions. And in addition, the equation of state utilized at highest densities and temperatures sets the conditions for such environments.

## ACKNOWLEDGMENTS

We want to thank all our collaborators with whom we investigated r-process sites and conditions, as well as everybody with whom we had enlightening discussions. These include Almudena Arcones, Shawn Bishop, Gabriele Cescutti, Cristina Chiappini, John Cowan, Khalil Faruqi, Brad Gibson, Maik Frensel, Chris Fryer, Samuel Giuliani, Yuhri Ishimaru, Thomas Janka, Oliver Just, Roger Käppeli, Oleg Korobkin, Karl-Ludwig Kratz, Karlheinz Langanke, Jim Lattimer, Matthias Liebendörfer, Andreas Lohs, Lucio Mayer, Gail McLaughlin, Tomislav Marketin, Dirk Martin, Gabriel Martinez-Pinedo, Francesca Matteucci, Nobuya Nishimura, Francesco Pannarale, Albino Perego, Marco Pignatari, Tsvi Piran, David Radice, Thomas Rauscher, Stephan Rosswog, Chris Sneden, Rebecca Surman, Tomoya Takiwaki, Masaomi Tanaka, Cristina Volpe, Shinja Wanajo, Christian Winteler, Meng-Ru Wu and many others. This research was supported by the Swiss SNF (via a regular research grant and a SCOPES project), an ERC Advanced grant from the European Commission (FISH), and the Russian Science Foundation (project No. 16-12-10519).

## LITERATURE CITED

1. Baade W, Zwicky F. *Physical Review* 46:76 (1934)
2. Hewish A, Okoye SE. *Nature* 207:59 (1965)
3. Özel F, Psaltis D, Narayan R, Santos Villarreal A. *Astrophys. J.* 757:55 (2012)
4. Hebel K, Lattimer JM, Pethick CJ, Schwenk A. *Astrophys. J.* 773:11 (2013)
5. Oertel M, Hempel M, Klähn T, Typel S. *ArXiv e-prints* (2016)
6. Hulse RA, Taylor JH. *Astrophys. J.* 195:L51 (1975)
7. Lattimer JM, Schramm DN. *Astrophys. J.* 192:L145 (1974)
8. Lattimer JM, Schramm DN. *Astrophys. J.* 210:549 (1976)
9. Symbalisty E, Schramm DN. *Astrophys. J.* 22:143 (1982)
10. Meyer BS, Schramm DN. 1988. In *Origin and Distribution of the Elements*, ed. GJ Mathews
11. Eichler D, Livio M, Piran T, Schramm DN. *Nature* 340:126 (1989)
12. Davies MB, Benz W, Piran T, Thielemann FK. *Astrophys. J.* 431:742 (1994)
13. Ruffert M, Janka HT, Schaefer G. *Astron. Astrophys.* 311:532 (1996)
14. Rosswog S, et al. *Astron. Astrophys.* 341:499 (1999)
15. Rosswog S, Davies MB, Thielemann FK, Piran T. *Astron. Astrophys.* 360:171 (2000)
16. Freiburghaus C, Rosswog S, Thielemann FK. *Astrophys. J.* 525:L121 (1999)
17. Panov IV, Thielemann FK. *Astronomy Letters* 30:647 (2004)
18. Panov IV, Korneev IY, Thielemann FK. *Astronomy Letters* 34:189 (2008)
19. Goriely S, Bauswein A, Janka HT. *Astrophys. J.* 738:L32 (2011)

20. Korobkin O, Rosswog S, Arcones A, Winteler C. *Mon. Not. R. Astron. Soc.* 426:1940 (2012)
21. Panov IV, Korneev IY, Lutostansky YS, Thielemann FK. *Physics of Atomic Nuclei* 76:88 (2013)
22. Bauswein A, Goriely S, Janka HT. *Astrophys. J.* 773:78 (2013)
23. Goriely S, et al. *Physical Review Letters* 111:242502 (2013)
24. Hotokezaka K, Kyutoku K, Shibata M. *Phys. Rev. D* 87:044001 (2013)
25. Rosswog S, et al. *Mon. Not. R. Astron. Soc.* 439:744 (2014)
26. Wanajo S, et al. *Astrophys. J.* 789:L39 (2014)
27. Just O, et al. *Mon. Not. R. Astron. Soc.* 448:541 (2015)
28. Goriely S, et al. *Mon. Not. R. Astron. Soc.* 452:3894 (2015)
29. Perego A, et al. *Mon. Not. R. Astron. Soc.* 443:3134 (2014)
30. Eichler M, et al. *Astrophys. J.* 808:30 (2015)
31. Martin D, et al. *Astrophys. J.* 813:2 (2015)
32. Mendoza-Temis JdJ, et al. *Phys. Rev. C* 92:055805 (2015)
33. Ramirez-Ruiz E, et al. *Astrophys. J.* 802:L22 (2015)
34. Hotokezaka K, Piran T, Paul M. *Nature Physics* 11:1042 (2015)
35. Just O, et al. *Astrophys. J.* 816:L30 (2016)
36. Radice D, et al. *Mon. Not. R. Astron. Soc.* 460:3255 (2016)
37. Roberts LF, et al. *Mon. Not. R. Astron. Soc.* 464:3907 (2017)
38. Oechslin R, Rosswog S, Thielemann FK. *Phys. Rev. D* 65:103005 (2002)
39. Oechslin R, Uryū K, Poghosyan G, Thielemann FK. *Mon. Not. R. Astron. Soc.* 349:1469 (2004)
40. Oechslin R, Janka HT, Marek A. *Astron. Astrophys.* 467:395 (2007)
41. Sekiguchi Y, Kiuchi K, Kyutoku K, Shibata M. *Phys. Rev. D* 91:064059 (2015)
42. Sekiguchi Y, et al. *Phys. Rev. D* 93:124046 (2016)
43. Kiuchi K, et al. *Phys. Rev. D* 92:124034 (2015)
44. Dessart L, et al. *Astrophys. J.* 690:1681 (2009)
45. Lehner L, et al. *Classical and Quantum Gravity* 33:184002 (2016)
46. Metzger BD, Fernández R. *Mon. Not. R. Astron. Soc.* 441:3444 (2014)
47. Surman R, McLaughlin GC, Hix WR. *Astrophys. J.* 643:1057 (2006)
48. Surman R, et al. *Astrophys. J.* 679:L117 (2008)
49. Surman R, et al. *Journal of Physics G Nuclear Physics* 41:044006 (2014)
50. Fernández R, Kasen D, Metzger BD, Quataert E. *Mon. Not. R. Astron. Soc.* 446:750 (2015)
51. Wu MR, Fernández R, Martínez-Pinedo G, Metzger BD. *Mon. Not. R. Astron. Soc.* 463:2323 (2016)
52. Malkus A, Kneller JP, McLaughlin GC, Surman R. *Phys. Rev. D* 86:085015 (2012)
53. Foucart F, et al. *Phys. Rev. D* 91:124021 (2015)
54. Malkus A, McLaughlin GC, Surman R. *Phys. Rev. D* 93:045021 (2016)
55. Zhu YL, Perego A, McLaughlin GC. *Phys. Rev. D* 94:105006 (2016)
56. Frensel M, Wu MR, Volpe C, Perego A. *ArXiv e-prints* (2016)
57. Hotokezaka K, Piran T. *Mon. Not. R. Astron. Soc.* 450:1430 (2015)
58. Rosswog S. *Astrophys. J.* 634:1202 (2005)
59. Wanajo S, Janka HT. *Astrophys. J.* 746:180 (2012)
60. Kyutoku K, Ioka K, Shibata M. *Phys. Rev. D* 88:041503 (2013)
61. Foucart F, et al. *Phys. Rev. D* 90:024026 (2014)
62. Mennekens N, Vanbeveren D. *Astron. Astrophys.* 564:A134 (2014)
63. Rosswog S, et al. *ArXiv e-prints* (2016)
64. Mumpower MR, Surman R, McLaughlin GC, Aprahamian A. *Progress in Particle and Nuclear Physics* 86:86 (2016)
65. Shibagaki S, et al. *Astrophys. J.* 816:79 (2016)
66. Bauswein A, Stergioulas N, Janka HT. *Phys. Rev. D* 90:023002 (2014)

67. Bauswein A, Stergioulas N, Janka HT. *European Physical Journal A* 52:56 (2016)
68. Li LX, Paczyński B. *Astrophys. J.* 507:L59 (1998)
69. Tanvir NR, et al. *Nature* 500:547 (2013)
70. Tanaka M, Hotokezaka K. *Astrophys. J.* 775:113 (2013)
71. Kasen D, Badnell NR, Barnes J. *Astrophys. J.* 774:25 (2013)
72. Grossman D, Korobkin O, Rosswog S, Piran T. *Mon. Not. R. Astron. Soc.* 439:757 (2014)
73. Wanderman D, Piran T. *Mon. Not. R. Astron. Soc.* 448:3026 (2015)
74. Fryer CL, et al. *Astrophys. J.* 812:24 (2015)
75. Hotokezaka K, et al. *Mon. Not. R. Astron. Soc.* 459:35 (2016)
76. Barnes J, Kasen D, Wu MR, Martínez-Pinedo G. *Astrophys. J.* 829:110 (2016)
77. Metzger BD. *Living Reviews in Relativity* 20:3 (2017)
78. Fernández R, Metzger BD. *Annual Review of Nuclear and Particle Science* 66:23 (2016)
79. Abbott BP, et al. *Physical Review Letters* 116:131103 (2016)
80. Roederer IU, et al. *Astrophys. J.* 791:32 (2014)
81. Sneden C, Cowan JJ, Gallino R. *Ann. Rev. Astron. Astrophys.* 46:241 (2008)
82. Roederer IU, et al. *Astrophys. J. Suppl.* 203:27 (2012)
83. Qian YZ, Wasserburg GJ. *Physics Reports* 442:237 (2007)
84. Honda S, et al. *Astrophys. J.* 643:1180 (2006)
85. Hansen CJ, Montes F, Arcones A. *Astrophys. J.* 797:123 (2014)
86. Roederer IU. *Astrophys. J.* 835:23 (2017)
87. Nishimura N, Takiwaki T, Thielemann FK. *Astrophys. J.* 810:109 (2015)
88. Nishimura N, et al. *Astrophys. J.* 836:L21 (2017)
89. Cayrel R, et al. *Nature* 409:691 (2001)
90. Thielemann FK. *Nature Physics* 11:993 (2015)
91. Suda T, et al. *Publ. Astron. Soc. Japan* 60:1159 (2008)
92. Suda T, et al. *Mon. Not. R. Astron. Soc.* 412:843 (2011)
93. Matteucci F, et al. *Mon. Not. R. Astron. Soc.* 447:326 (2015)
94. Macias P, Ramirez-Ruiz E. *ArXiv e-prints* (2016)
95. Chruslinska M, Belczynski K, Bulik T, Gladysz W. *ArXiv e-prints* (2016)
96. Argast D, Samland M, Thielemann FK, Qian YZ. *Astron. Astrophys.* 416:997 (2004)
97. Cescutti G, et al. *Astron. Astrophys.* 577:A139 (2015)
98. van de Voort F, et al. *Mon. Not. R. Astron. Soc.* 447:140 (2015)
99. Shen S, et al. *Astrophys. J.* 807:115 (2015)
100. Wehmeyer B, Pignatari M, Thielemann FK. *Mon. Not. R. Astron. Soc.* 452:1970 (2015)
101. Hirai Y, et al. *Astrophys. J.* 814:41 (2015)
102. Mennekens N, Vanbeveren D. *Astron. Astrophys.* 589:A64 (2016)
103. Cowan JJ, et al. *Astrophys. J.* 627:238 (2005)
104. Cohen JG, Huang W. *Astrophys. J.* 701:1053 (2009)
105. Jablonka P, et al. *Astron. Astrophys.* 583:A67 (2015)
106. Simon JD, et al. *Astrophys. J.* 802:93 (2015)
107. Tsujimoto T, Nishimura N. *Astrophys. J.* 811:L10 (2015)
108. Ji AP, Frebel A, Chiti A, Simon JD. *Nature* 531:610 (2016)
109. Ji AP, Frebel A, Simon JD, Chiti A. *Astrophys. J.* 830:93 (2016)
110. Ishimaru Y, Wanajo S, Prantzos N. *Astrophys. J.* 804:L35 (2015)
111. Beniamini P, Hotokezaka K, Piran T. *Astrophys. J.* 832:149 (2016)
112. Metzger BD, et al. *Mon. Not. R. Astron. Soc.* 406:2650 (2010)
113. Berger E, Fong W, Chornock R. *Astrophys. J.* 774:L23 (2013)
114. Yang B, et al. *Nature Communications* 6:7323 (2015)
115. Lippuner J, Roberts LF. *Astrophys. J.* 815:82 (2015)
116. Davis AM, McKeegan KD (2014). Short-Lived Radionuclides and Early Solar System Chronology. 361–395

117. Thielemann FK, Hirschi R, Liebendörfer M, Diehl R. 2011. In *Lecture Notes in Physics, Berlin Springer Verlag*, eds. R Diehl, DH Hartmann, N Prantzos, vol. 812 of *Lecture Notes in Physics, Berlin Springer Verlag*
118. Wanajo S, Janka HT, Müller B. *Astrophys. J.* 774:L6 (2013)
119. Knie K, et al. *Physical Review Letters* 93:171103 (2004)
120. Wallner A, et al. *Nature* 532:69 (2016)
121. Fimiani L, et al. *Physical Review Letters* 116:151104 (2016)
122. Ludwig P, et al. *Proceedings of the National Academy of Science* 113:9232 (2016)
123. Wallner A, et al. *Nature Communications* 6:5956 (2015)
124. Woosley SE, Hoffman RD. *Astrophys. J.* 395:202 (1992)
125. Roberts LF, Woosley SE, Hoffman RD. *Astrophys. J.* 722:954 (2010)
126. Farouqi K, et al. *Astrophys. J.* 712:1359 (2010)
127. Freiburghaus C, et al. *Astrophys. J.* 516:381 (1999)
128. Nomoto K, Thielemann FK, Miyaji S. *Astron. Astrophys.* 149:239 (1985)
129. Hix WR, Thielemann FK. *Journal of Computational and Applied Mathematics* 109:321 (1999)
130. Timmes FX. *Astrophys. J. Suppl.* 124:241 (1999)
131. Panov IV, et al. *Astron. Astrophys.* 513:A61 (2010)
132. Kelic A, Ricciardi MV, Schmidt KH. 2008. In *Dynamical Aspects of Nuclear Fission*, eds. J Kliman, MG Itkis, Š Gmuca
133. Möller P, Nix JR, Myers WD, Swiatecki WJ. *Atomic Data and Nuclear Data Tables* 59:185 (1995)
134. Duffo J, Zuker AP. *Phys. Rev. C* 52:R23 (1995)
135. Möller P, Myers WD, Sagawa H, Yoshida S. *Physical Review Letters* 108:052501 (2012)
136. Goriely S, Chamel N, Pearson JM. *Phys. Rev. C* 88:024308 (2013)
137. Wang N, Liu M. 2013. In *Journal of Physics Conference Series*, vol. 420 of *Journal of Physics Conference Series*
138. Möller P, Pfeiffer B, Kratz KL. *Phys. Rev. C* 67:055802 (2003)
139. Marketin T, Huther L, Martínez-Pinedo G. *Phys. Rev. C* 93:025805 (2016)
140. Panov IV, Lutostansky YS, Thielemann FK. *Nuclear Physics A* 947:1 (2016)
141. Martínez-Pinedo G, Fischer T, Lohs A, Huther L. *Physical Review Letters* 109:251104 (2012)
142. Roberts LF, Reddy S, Shen G. *Phys. Rev. C* 86:065803 (2012)
143. Kodama T, Takahashi K. *Nuclear Physics A* 239:489 (1975)
144. Qian YZ, Woosley SE. *Astrophys. J.* 471:331 (1996)
145. Kitaura FS, Janka HT, Hillebrandt W. *Astron. Astrophys.* 450:345 (2006)
146. Janka HT, Müller B, Kitaura FS, Buras R. *Astron. Astrophys.* 485:199 (2008)
147. Wanajo S, et al. *Astrophys. J.* 695:208 (2009)
148. Wanajo S, Janka HT, Müller B. *Astrophys. J.* 726:L15 (2011)
149. Fujimoto Si, Nishimura N, Hashimoto Ma. *Astrophys. J.* 680:1350 (2008)
150. Ono M, et al. *Progress of Theoretical Physics* 128:741 (2012)
151. Winteler C, et al. *Astrophys. J.* 750:L22 (2012)
152. Mösta P, et al. *Astrophys. J.* 785:L29 (2014)
153. Mösta P, et al. *Nature* 528:376 (2015)
154. Greiner J, et al. *Nature* 523:189 (2015)